(2)

REPORT DOCUMENTATION PAGE

Form Approved
OMB No. 0704-0188

1. AGENCY USE ONLY (Leave blank)	2. REPORT DATE	3. REPORT TYPE AND DATES COVERED
	1/20/94	Interim 6/93 - 12/93

4. TITLE AND SUBTITLE

Pitting Corrosion of Titanium

5. FUNDING NUMBERS

N00014-91-J-1927

R & T Code 413V001

6. AUTHOR(S)

Norberto Casillas, Steven J. Charlebois
William H. Smyrl and Henry S. White

7. PERFORMING ORGANIZATION NAME(S) AND ADDRESS(ES)

Department of Chemistry
Henry Eyring Building
University of Utah
Salt Lake City, Utah 84112

8. PERFORMING ORGANIZATION REPORT NUMBER

28

9. SPONSORING/MONITORING AGENCY NAME(S) AND ADDRESS(ES)

Office of Naval Research
800 North Quincy Street
Arlington, Virginia

10. SPONSORING/MONITORING AGENCY REPORT NUMBER

11. SUPPLEMENTARY NOTES

12a. DISTRIBUTION/AVAILABILITY STATEMENT

Unclassified/Unlimited

DISTRIBUTION STATEMENT A
Approved for public release;
Distribution Unlimited

12b. DISTRIBUTION CODE

13. ABSTRACT (Maximum 200 words)

The breakdown of native and anodically -grown oxide films on Ti electrodes is investigated by scanning electrochemical microscopy (SECM), video microscopy, transmission electron microscopy and voltammetry. SECM is used to demonstrate that the oxidation of Br^- on Ti occurs at microscopic surface sites (10 - 50 μm diameter, 30 sites/cm^2) that are randomly positioned across the oxide surface. After determining the position of the active sites for Br^- oxidation, breakdown of the oxide is initiated by increasing the electrode potential to more positive values. Direct correspondence is observed between the location of the electroactive sites and corrosion pits, indicating that oxide breakdown is associated with a localized site of high electrical conductivity. The potential at which pitting is observed in voltammetric experiments is found to be proportional to the average oxide thickness, for values ranging between 20 and 100 Å, indicating that breakdown is determined either by the magnitude of the electric field within the oxide or by the interfacial potential at the oxide/Br^- solution interface. Pitting occurs at significantly lower potentials in Br^- solutions than in Cl^- solutions, suggesting a strong chemical interaction between the TiO_2 surface and Br^-. A mechanism of oxide breakdown is proposed that is based on the potential-dependent chemical dissolution of the oxide at microscopic surface sites.

14. SUBJECT TERMS	15. NUMBER OF PAGES
Scanning Electrochemical Microscopy; Corrosion Pitting; Titanium	16. PRICE CODE

17. SECURITY CLASSIFICATION OF REPORT	18. SECURITY CLASSIFICATION OF THIS PAGE	19. SECURITY CLASSIFICATION OF ABSTRACT	20. LIMITATION OF ABSTRACT
Unclassified	Unclassified	Unclassified	

NSN 7540-01-280-5500

Standard Form 298 (Rev. 2-89)
Prescribed by ANSI Std. Z39-18
298-102

OFFICE OF NAVAL RESEARCH

Contract N00014-91-J-1927

R&T Code 413v001

Technical Report No. 28

PITTING CORROSION OF TITANIUM

by

NORBERTO CASILLAS, STEVEN J. CHARLEBOIS,
WILLIAM H. SMYRL AND HENRY S. WHITE

Prepared for Publication in

Journal of the Electrochemical Society

University of Utah
Department of Chemistry
Salt Lake City, UT 84112

December 16, 1993

PITTING CORROSION OF TITANIUM

Norberto Casillas, Steven Charlebois, William H. Smyrl
Department of Chemical Engineering & Materials Science
University of Minnesota
Minneapolis, MN 55455

and

Henry S. White
Department of Chemistry
University of Utah
Salt Lake City, UT 84112

ABSTRACT. The breakdown of native and anodically-grown oxide films on Ti electrodes is investigated by scanning electrochemical microscopy (SECM), video microscopy, transmission electron microscopy, and voltammetry. SECM is used to demonstrate that the oxidation of Br^- on Ti occurs at microscopic surface sites (10 - 50 μm diameter, 30 sites/cm^2) that are randomly positioned across the oxide surface. After determining the position of the active sites for Br^- oxidation, breakdown of the oxide is initiated by increasing the electrode potential to more positive values. Direct correspondence is observed between the location of the electroactive sites and corrosion pits, indicating that oxide breakdown is associated with a localized site of high electrical conductivity. The potential at which pitting is observed in voltammetric experiments is found to be proportional to the average oxide thickness, for values ranging between 20 and 100 A, indicating that breakdown is determined either by the magnitude of the electric field within the oxide or by the interfacial potential at the oxide/Br^- solution interface. Pitting occurs at significantly lower potentials in Br^- solutions than in Cl^- solutions, suggesting a strong chemical interaction between the TiO_2 surface and Br^-. A mechanism of oxide breakdown is proposed that is based on the potential-dependent chemical dissolution of the oxide at microscopic surface sites.

Submitted to *J. Electrochem. Soc.*, July, 1993.

INTRODUCTION. The chemical stability of Ti is due to the formation of a thin TiO_2 film on the surface. The oxide film, which is ~20Å thick in the native state, is chemically inert in air and most aqueous solutions, and serves to separate the highly reactive underlying Ti metal from corrosive environments. Breakdown of the TiO_2 film in aqueous halide solutions occurs rapidly when the potential of the metal is increased to values above ~1V, the exact potential being dependent on the identity of the halogen ion. Following oxide breakdown, exposure of the Ti substrate results in rapid growth of a corrosion pit.

The most detailed investigations of corrosion pitting of Ti in halide solutions are described by Dugdale and Cotton[1] and by Beck.[2,3,4]. One of several findings of these earlier studies is the tendency for Ti electrodes to pit at significantly lower potentials in Br^- solutions than in either I^- or Cl^- solutions. To our knowledge, an explanation of this observation has not yet been described.

In a preliminary report from our laboratories[5], the breakdown of 50 Å-thick oxide films on Ti electrodes immersed in aqueous solutions containing Br^- was shown to occur at randomly positioned, microscopic surface sites that were identified by scanning electrochemical microscopy (SECM) prior to corrosion pitting. A key finding of this investigation was that the site of oxide breakdown correlated with a highly localized surface activity for Br^- oxidation. These studies suggested that the electrical conductivity of the TiO_2 film is highly non-uniform, and that this spatial heterogeneity is associated with the mechanism of oxide film breakdown. Electron tunneling spectroscopy of the electrodes, employing a scanning tunneling microscope, more directly demonstrated local variations in the conductivity of the oxide, albeit for

reasons that are not understood, but that are probably related to variations in the structure (e.g, defect density) or stoichiometry of the film[6].

In the present report, a detailed description of SECM imaging of Ti electrodes in Br^- solutions is described. In addition to extending our previous analyses of the localized oxidation of Br^- at microscopic surface sites, and the correlation of such sites as precursors for pitting, we now report measurements of the rate of Br^- oxidation and the potential of oxide breakdown as a function of the oxide film thickness. The rate of Br^- oxidation at precursor sites for oxide breakdown is shown to decrease with increasing film thickness, concurrent with an increase in the potential necessary to initiate pitting. The results suggest that the above mentioned acceleration of oxide breakdown in Br^- solutions is related to a potential-dependent chemical interaction between the oxide and the solution anion. A mechanism of oxide breakdown is proposed that is consistent with the observed dependence of breakdown on the film thickness, the chemical specificity to Br^-, and the local spatial variations in the electrochemical activity for Br^- oxidation prior to pitting. In addition to these studies, a method is described for preparing free-standing 50 Å-thick TiO_2 films.

EXPERIMENTAL

Preparation of Ti Electrodes. Ti electrodes were constructed from 25 μm thick, ~5 mm x 25 mm rectangular samples of 99.98% commercially pure Ti (Johnson Matthey, Ward Hill, MA). A copper wire was attached to the foil using silver epoxy (Acme, Inc). The copper wire and silver epoxy were sealed into the end of a glass pipette with epoxy (Dexter, Inc), exposing the sides and the edges of the Ti sample.

Ti electrodes were etched in a solution containing 2% (by vol.) HF (Mallinckrodt Inc.), 4% HNO_3 (Fisher Scientific Inc.) and 94% H_2O by wiping the surface with a cotton swab that was wetted with the etching solution. The electrodes were rinsed with deionized water and dried in air. Anodic growth of oxide was performed in a 0.05 M H_2SO_4 solution. The electrode was immersed in the 0.05 M H_2SO_4 solution until an open-circuit potential of -0.25 V vs a saturated calomel electrode (SCE) was obtained. The potential of the Ti electrode was then scanned from the open-circuit value to the desired oxide growth potential at a rate of 1 mV/s. A typical oxide growth curve is shown in Fig. 1. The thickness of the oxide film was determined using a calibration plot of ellipsometrically-measured thickness (t) vs final growth potential, reported by Ohtsuka et al.[7] The calibration plot was established using a growth procedure similar to that employed in the present study.

All voltammetric measurements were performed using a conventional 3-electrode cell configuaration, with a Pt counter electrode and a SCE reference electrode.

Scanning Electrochemical Microscopy. Fig. 2 shows a schematic of the scanning electrochemical microscope (SECM). A custom-built Teflon cell, used in previous iontophoresis/SECM experiments[8-12], was adapted for imaging Ti electrodes. Four ports, positioned one on each side of the corrosion cell, held two platinum auxiliary electrodes and two SCE reference electrodes.

The SECM scanning tip was an 8 μm diameter carbon fiber (Johnson Matthey) insulated with polyphenylene oxide except at the very tip. The method of preparing the carbon fiber followed the procedure of Potje-Kamloth et al.[13] The upper 10 mm of a 20 mm-long carbon fiber was inserted into a 3 mL glass microcapillary (Drummond Scientific Inc.) and sealed at the end with

epoxy (Dexter Inc.). To provide a conductive path to the scanning tip, a 0.25 mm-diameter tungsten wire (Johnson Matthey Inc.) was inserted into the end of the microcapillary and attached to the carbon fiber with silver epoxy. Polyphenylene was electrodeposited on the lower portion of the fiber from a 40:60 H_2O/methanol solution containing 0.25 M 2-allylphenol (Aldrich, Inc.), 0.4 M ammonium hydroxide (Mallinckrodt Inc), and 0.2 M 2-butoxyethanol (Fisher Scientific Inc.). A 3-electrode cell configuration was used to deposit polyphenylene oxide on the carbon fiber for 2 minutes at a potential of 4 V vs SCE. The insulated carbon fiber was then rinsed with a 40/60 mixture of H_2O/methanol and cured at 130 °C for 30 min. The active area of the carbon fiber microelectrode was exposed by cutting the insulated fiber using a razor blade. The electrochemical activity of the fiber was tested by cyclic voltammetry in a 0.1 M $K_3Fe(CN)_6$ solution prior to use in SECM imaging.

The potential of the Ti electrode and SECM scanning tip were controlled independently using two potentiostats, both operating in a conventional 3-electrode configuration. A Pine Instrument RDE4 potentiostat was used to control the potential of the Ti electrode. A previously described custom-built low-current potentiostat was used to control the potential of the SECM scanning tip.[9]

The typical procedure for obtaining a SECM image is as follows. First, the Ti electrode is immersed in the 1M KBr, 0.05M H_2SO_4 solution without applying a potential bias to either the SECM scanning tip or the sample. The SECM tip is lowered until it touches the Ti surface, producing a slight bend in the carbon fiber. The tip is then slowly raised until it is straightened. This position is taken as the vertical zero position ($z = 0$). From the zero point, the carbon fiber is moved away from the Ti surface until a gap of approximately 10 - 20 μm is established. After verifying free movement of the tip in the x-y plane, the

potential of the SECM tip and sample are set to constant values and the SECM tip is scanned in the x-y plane. The tip is scanned at a rate of 40 μ m/s.

SECM images are constructed by plotting the current measured at the tip vs the position of the tip as it is rastered in the x-y plane. Eight hundred data points are collected during each line scan in the x direction; every 4 consecutive data points are averaged resulting in 200 stored data points per scan. Low-resolution survey images are acquired by incrementing the tip in the y direction by 100 μm after every line scan. Higher-resolution images were acquired by incrementing the tip in the y direction by ~10 μm after each line scan. Acquisition of a 400 x 400 μm^2 image using the latter mode requires ~15 minutes.

Only high resolution images are reported in this article. However, the low-resolution survey scans are especially useful in initially identifying the positions of electroactive sites on the Ti surface, as well as for rapidly collecting data for the statistical analysis of the number of electroactive sites on a large area sample. Identification of the electroactive sites was also greatly facilitated by converting the SECM tip reponse to an audio signal, Fig. 2. The frequency of the audio reponse was proportional to the tip current, alerting the experimentalist, in real time, that the SECM tip was above a site of high electrochemical activity. Since the number density of sites that occur on the samples investigated was extremely low (~30 per cm^2, vide infra), the low resolution method of on-line detection was found to be particularly useful, reducing the analysis time by an order of magnitude. Once an electroactive site had been located, the higher resolution imaging mode was employed to obtain the images presented in this article. Data acquisition and x-y positioning are controlled by an IBM XT microcomputer as previously

described. Stored data are replotted in 16-level gray scale format using a Macintosh II-ci computer.

The Ti electrode and the scanning tip are monitored during imaging using a video camera (JVC Inc.) equipped with a 50 X magnification zoom-lens; video images are recorded using a VHS video recorder (JVC Inc.).

Surface analyses of free-standing TiO_2 films. Transmission electron microscopy (JEOL 100CX electron microscope), x-ray photoelectron spectroscopy (Perkin-Elmer Phi 5400 ESCA), and Auger electron spectroscopy (Physical Electronics) were used for analysis of free-standing 50 Å-thick TiO_2 films. Free standing films were prepared by biasing a Ti electrode (t = 50Å) in a 1 M KBr, 0.05 M H_2SO_4 solution at a potential sufficiently positive (~3-5 V vs SCE) to initiate the growth of 3 - 4 active pits. Rapid dissolution of the Ti metal beneath the oxide film occurred without further initiation of active pits, as readily determined by video microscopy (vide infra). After ~10 minutes, all of the Ti electrode had dissolved, yielding 2 (back and front sides) large area 50 Å TiO_2 films. The films spontaneously collapsed and broke into smaller pieces; however, millimeter-size pieces of the TiO_2 films were carefully collected from the solution using a 200-mesh gold (Electron Microscopy Sciences Inc.) or 400-mesh platinum (Asar Co.) microscope grids. The films were then immersed in H_2O to remove any remaining KBr solution. The oxide films were collected from the H_2O using microscope grids and stored in a desiccator for 48 hours prior to surface analyses.

RESULTS AND DISCUSSION.

Voltammetric Behavior of Ti Electrodes. Titanium is susceptible to pitting corrosion in aqueous solutions containing Br^- over a wide range of solution

pH[14]. Our experiments are limited to investigations of Ti electrodes with either a native or anodically-grown oxide film, immersed in a 1 M KBr, 0.05 M H_2SO_4 solution (pH = 1.05) that was exposed to the ambient environment. All references to Br^--containing solutions refer to this specific solution composition. All electrode potentials are referenced to the SCE.

Fig. 3 shows the voltammetric behavior (scan rate = 1.0 mV/s) of Ti electrodes immersed in the Br^- solution for several different oxide thicknesses. The potential at which oxide breakdown occurs, E_p, is readily identified by an abrupt increase in the current density near the end of the positive scan. Visual inspection of the electrode surface immediately after the onset of pitting showed the presence of several large corrosion pits. Fig. 3 also shows that E_p shifts to positive potentials with increasing oxide thickness.

The voltammetric response of Ti electrodes with oxide thicknesses, t, between 40 and 70 Å also exhibited a broad anodic wave in the voltammetric curve between 1.2 V to 2 V. This wave corresponds to the oxidation of Br^- at the TiO_2 surface, and is completely absent in solutions containing only H_2SO_4 (compare Fig. 1 and 3). In one set of experiments, the amount of electrogenerated Br_2 present in the solution was periodically measured by UV-visible spectroscopy and found to be in good agreement (within 5%) with the value calculated by integration of the charge under the anodic wave.

Br^- oxidation is insignificant for oxide films thicker than ~70 Å, as indicated by the absence of the anodic wave centered between 1.2 and 2 V. For oxide films thinner that ~40 Å, the onset of pitting and Br^- oxidation occur at approximately the same potential, as shown in Fig. 3 for electrodes coated with a native oxide and a 30 Å-thick anodic oxide.

For electrodes with oxide films of intermediate thickness, e.g., t ~ 50 Å, the anodic wave corresponding to Br^- oxidation decays to background current

levels when the potential is more positive that ~1.6 V. Thus, the i-V curves in Fig. 3 do not represent steady-state responses. If the potential of the electrode is scanned repeatedly between 0 and 2 V, the size of the anodic wave is rapidly diminished. Our interpretation of these findings is that electrode potentials more positive that 1.6 V result in passivation of the surface towards Br^- oxidation. The fact that the Br^- oxidation wave is not observed for $t > 70$ Å, indirectly indicates that an increase in the thickness of the 50 Å-thick oxide layer, beginning at ~1.6 V, is responsible for the observed time-dependent decrease in rate of Br^- oxidation.

A low power microscope was used to determine the number of pits on the TiO_2 surface. Analyses of 25 Ti electrodes for each oxide thickness, made for the first two minutes after the first pit appeared, yielded values of 20 ± 10 pits/cm^2 for t = 20 Å (native oxide), 6 ± 3 for t = 30Å, 5 ± 2 for t = 50 Å and 3 ± 2 for t = 90 Å. The larger number density of pits observed for the native oxide films suggests the existence of a larger number of precursor sites for oxide breakdown. The existence of these precursor sites is demonstrated using SECM, as discussed in a later section.

Fig. 4 shows the dependence of the breakdown potential, E_p, on the oxide film thickness, *t*. Each data point represents at least 10 independent measurements of E_p. The data indicate that E_p has an approximately linear dependence on the oxide thickness, a point that we shall address later in the discussing the mechanism of pitting. The dependence of E_p on scan rate has not been investigated; however, we note that pitting is observed to occur at substantially lower potentials than the values indicated in Fig. 4, if the electrode is biased at a constant potential for extended periods (e.g., 40 minutes at 1.5 V for a 50 Å thick film). Thus, the reported values of E_p most likely are affected by the kinetics of the breakdown reaction.

The temperature dependence of the pitting potential was briefly investigated. Fig. 5 shows voltammetric curves obtained at 0 and 22 °C for electrodes passivated by a native oxide film. In qualitative agreement with the more extensive studies of Beck[3], the onset of pitting in Br^- is shifted positive by 2 ± 1 V at the lower temperature, suggesting that pitting is a thermally activated process.

Active Pit Growth and Free-Standing Oxide Films.

The growth of active pits on a Ti electrode (t = 50Å) was recorded using video microscopy. Fig. 6 shows an example of a time-lapse sequence showing pit nucleation and growth over a ~2 minute period. In this experiment, the electrode was scanned at 1 mV/s to the pitting potential (~2.5 V, as noted by a sudden increase in current). The growth of the pit results in a steady stream of gas bubbles that emerges from a singular point on the surface (Fig. 6). During the next 2 minutes, pits nucleate and growth at several locations on the surface, each producing a stream of small bubbles. A particularly interesting feature of pit growth is that as the metal rapidly dissolves, a thin oxide "veil" is generated that covers the region of metal dissolution. Using a video camera with a 50 X magnification lens, the gas bubbles are observed to flow through a small circular opening in the oxide veil, which is located at the point of oxide breakdown. Oxide veils over several large pits (~2 mm diameter) can be seen in Fig. 6. The openings in the oxide film, which are not apparent in the reproductions of the low-resolution micrographs, have diameters on the order of 50 μm.

Fig. 7 shows a schematic picture of the pit geometry (not drawn to scale) and the processes occurring within the pit. Ti dissolution is rapid within the pit cavity as noted by the moving boundary of the metal/solution interface.

The gaseous products, which have not been analyzed, can be seen in the video tapes to flow radially from the metal/solution interface towards the center of the circular-shaped pit, escaping through the small opening in the oxide film. Continued metal dissolution leads to overlapping pits (Fig. 6). Eventually, the pits extend to the edges of the electrode, resulting in complete dissolution of the electrode. At the end of the experiment, two 50 Å-thick free-standing oxide films (corresponding to the front and back oxide layers) remain attached to the glass tubing and epoxy that initially supported the (dissolved) electrode. The films tend to collapse during attempts to remove them from the solution. However, millimeter-size pieces can be collected from the solution (see *Experimental Section*) and examined by ex-situ microscopy and surface spectroscopy.

Fig. 8 shows a TEM micrograph of a free-standing 50 Å TiO_2 film produced by the above method. The oxide film is polycrystalline with an average grain size of 1.5 μm^2. Electron diffraction patterns of the free-standing films indicate that individual grains are crystalline. Auger electron spectroscopy (AES) of the films yield signals for Ti, O, C and S, the strongest signals at 390 eV and 505 eV corresponding to Ti and O, respectively [15]. The presence of C and S signals likely correspond to surface contamination. Results from X-ray photoelectron spectroscopy are consistent with the AES data. In addition, AES depth profiling of the oxide films did not show peaks corresponding to Br, indicating that there was very little, if any, diffusion of Br^- into the oxide film during the pitting experiment.

Scanning Electrochemical Microscopy (SECM). In a previous report[5], SECM was used to demonstrate large spatial variations in the rate of oxidation of Br^- on Ti electrodes. The SECM tip (an 8 µm-diameter carbon fiber microelectrode)

was rastered across the Ti surface while being held at a potential sufficiently negative of the standard redox potential of the Br^-/Br_2 couple to reduce Br_2 at the mass-transport limited rate, Fig. 9. The rate of Br_2 reduction is a direct measure of the local concentration of Br_2 at the surface of the Ti electrode. Thus, variations in the cathodic current at the SECM tip, as a function of the tip position, reflect local variations in the rate of Br^- oxidation on the Ti surface.

Only electrodes covered by 50 Å-thick anodically-grown oxide films were investigated in the SECM experiments. Oxide films of thickness less than 40Å tended to break down at potentials that significantly overlap with Br^- oxidation, Fig. 3, making it impossible to detect Br_2 generation prior to pitting. On the other hand, Br^- oxidation is immeasurably slow on Ti electrodes that have oxide films of thickness greater than 70 Å. For the intermediate oxide thicknesses, Br^- oxidation is sufficiently fast that it can be detected in the SECM experiments, and since Br_2 is electrogenerated at potentials well-below the pitting potential at 50Å thick oxide, the surface can be readily imaged prior to breakdown. However, as noted above, if an electrode with a 50Å thick oxide is held at a constant potential within the potential region where Br^- oxidation occurs (e.g., 1.5 V), oxide breakdown will occur after an induction period of ~40 minutes. For this reason, a relatively large tip scan rate of 40 μm/s was used to acquire images prior to breakdown. As shown below, this rather fast scan speed resulted in some distortion of the SECM images due to convective flow induced by the tip.

Fig. 10 shows SECM images (400 x 400 μm^2) for 4 different Ti electrodes (t = 50Å). The SECM tip was maintained at a constant potential of 0.6 V and positioned ~20 μm above the surface. When the Ti surface was baised at potentials below 1.0 V, SECM images were essentially featureless and the tip current was of the magnitude of ~0.1 nA. At potentials between 1.0 and 2.0 V,

SECM images revealed a number of microscopic sites where the Br_2 concentration was large. For example, Fig. 10 (a) illustrates a typical SECM image of an electroactive site on the TiO_2 surface. The sample was held at a potential of 1.3 V during the scanning. The maximum current detected in this area was 1.45 nA, well above the background current of 0.1 nA. The large differences between the maximum and the background currents clearly demonstrates that the oxidation of Br^- does not occur uniformly across the surface.

The number of surface sites active for Br^- oxidation on the anodic surfaces is small. From low resolution survey scans on several electrodes, a value of 30 ± 10 sites/cm^2 was determined for the 50 Å thick TiO_2 films.

To estimate the size of the electroactive sites on the Ti electrode, a 25 μm-diameter Pt microdisk electrode was imaged by SECM in the same Br^- solution. The potentials for the SECM tip and Pt disk were maintained at 0.6 V and 1.0, respectively, and the tip was positioned ~20 μm above the Pt surface. Fig. 11 shows a typical image of the Pt disk. Comparison of this image with the SECM images in Fig. 10 demonstrates that the dimensions of the electroactive sites on the Ti electrode are comparable to that of the Pt disk. We estimate that the diameters of the electroactive sites range from 10 to 50 μm. The rate of Br^- oxidation, as estimated from the magnitude of the SECM tip current, is an order of magnitude larger on the Pt disk that for the most active sites on the Ti electrodes. Although the rate of Br^- oxidation at the microscopic sites is sufficiently large to allow their detection by SECM, the smaller currents indicates that the reaction proceeds at a kinetically- controlled rate. This finding is not surprising in view of the fact that the average thickness of the oxide film is 50 Å.

Each of the images in Figs. 11 and 12 are slightly distorted due to the high tip scan speed employed in these studies. The tip movement causes the fluid to flow in the direction of the scan, resulting in nonspherical concentration profiles around the Pt disk or electroactive sites on Ti, as is evident in the images. The effect is pronounced in the 1.0 M Br^- solutions, where a relatively dense layer of Br_2 is generated between the tip and substrate.

The SECM image contrast is a function of the potential applied to the Ti substrate, due to the potential dependence of Br^- oxidation on this substrate. Fig. 12 shows a set of four images of an electroactive site obtained at different potentials. Fig. 12 (a) shows the image of the active site at a potential of 1.3 V, with a maximum current of 0.16 nA, and a detected background current of 0.09 nA. Fig. 12 (b) shows the same area taken 13 minutes later at a potential of 1.4 V. The maximum current has increased to 0.18 nA. Fig. 12 (c) shows the same area scanned at a potential of 1.56 V. The current at the center of the active site increased to 0.24 nA. Fig. 12 (d) shows an image of the same area taken 40 minutes later at the same potential. Here, the maximum current has decreased to 0.18 nA, due to slow passivation of the surface, as previously discussed.

Fig. 13 shows a comparison between a voltammetric curve obtained for a 50 Å thick film at 1 mV/s (Fig. 3), and a i-V curve constructed from values of the maximum SECM tip current measured above an electroactive site. Both curves display similar shapes, with a maximum current at ~1.6 V.

Proposed Pitting Mechanism.

The mechanism for oxide breakdown and pitting must be consistent with the following experimental observations:

I. The microscopic sites at which breakdown occurs are electrochemically active. It therefore follows that the electrical conductivity of the oxide is high at these sites relative to the surrounding film.

II. Oxide breakdown occurs at more positive potentials with increasing average oxide film thickness.

III. Oxide breakdown occurs at significantly lower potentials in Br^- solutions ($E_p \leq 5$ V) relative to Cl ($E_p \geq 10$ V), as previously demonstrated by Dugdale and Cotton[1] and by Beck[2,3,4]. We have confirmed their results using Ti electrodes prepared in our laboratory.

Observation I clearly indicates that sites of oxide breakdown have a distinctly different structure or chemical composition in comparison to the average properties of the oxide film. For this reason, there is no need to discuss the breakdown mechanism in terms of stoichastic events. Observation II suggests that oxide breakdown occurs *either* when the electric field within the film exceeds a critical strength or when the potential at the TiO_2/solution interface exceeds a critical value. Both the field within the oxide and the interfacial potential will increase as the electrode potential is increased to positive values[16].

The chemical specificity of breakdown to solutions containing Br^- clearly eliminates any mechanism involving simple electrical or thermal

breakdown, as occurs in metal/dielectric/metal structures.[15] Such a mechanism would result in similar behavior for all of the halides. Beck's observation that the pitting potential has different temperature dependencies in Br^- and I^- solutions further suggests that the mechanism of pitting in solutions containing these halide ions may be completely different.

The involvement of the anion, coupled with the dependence of the pitting potential on oxide thickness, suggest a potential-dependent chemical dissolution of the outermost layer of the oxide in the presence of Br^-. Ti^{+4} readily forms a number of soluble oxo halide salts in acid solutions. We speculate that chemisorption of Br^- would be most pronounced at positive potentials, promoting the formation of Ti-Br bonds at the oxide/solution interface and subsequently, oxide dissolution.

The dependence on E_p on film thickness is the consequence of a larger potential drop occurring within the thicker films, i.e., for a constant applied potential, the potential at the oxide/solution interface would be less positive for a thicker film, resulting in a decrease in the concentration, or chemisorption, of Br^- at the interface[16]. The breakdown of the film, as is indicated by the abrupt increase in the current density (Fig. 3), would be anticipated based on this mechanism as a result of the rapid increase in the interfacial potential as the film became thinner.

Fig. 14 schematically depicts the various processes that occur during a voltammetric experiment and that lead to oxide breakdown. Based on SECM images of the Ti electrodes, the oxide film contains a low number density of sites (~30 sites/cm^2) that possess sufficient electrical conductivity for Br^- oxidation to occur at relatively fast rate. In Fig. 14, these sites have been depicted as a region where the insulating nature of the oxide is compromised, without regard to the physical or chemical properties of the oxide at the

microscopic site. For a 50 Å-thick oxide film, the following sequence of events appear to occur during a voltammetric scan (e.g., Fig. 3 for t = 50Å). Very little current flows at potentials negative of the redox potential of the Br^-/Br_2 couple (Fig. 14a). As the potential is biased to values positive of ~1.2 V, Br^- is rapidly oxidized at the microscopic sites (Fig. 14b). This process continues at higher potentials until the conductivity of the microscopic sites is reduced, most likely due to thickening of the oxide film (Fig. 14c). We note that a local increase in the oxide thickness at the microscopic sites, without an increase in the average film thickness, is sufficient to cause the passivation of the surface towards Br^- oxidation. Between ~2 and 3 V, Br^- is strongly chemisorbed (Fig. 14 d) leading to dissolution of the film and the growth of a pit.

The results presented here show that precursor sites for pitting of Ti may be identified with SECM. Further work will be needed to determine how precursor sites are formed as a function of surface pretreatment, film formation and processing, and the electrolyte chemistry. The results also enable further work to be done on the precursor sites themselves to characterize their unique susceptibility to breakdown. The susceptibility is undoubtedly associated with defect structures in the oxide film, but the type of defect is not revealed by the present study. Inclusions, mechanically formed defects, and structural defects due to crystallographic termination are important for bulk and surface electronic properties of TiO_2. Other types of defects, such as line defects at steps and terraces, three dimensional defects at oxide crystallite grain boundaries, and crystallographic shear plane array defects are expected to influence the bulk and surface as well[17-20]. High concentrations of these types of defects may increase the electronic

conductivity. Identifying the type of defect, how it is formed, and especially how it may be eliminated, are of fundamental and technological importance.

ACKNOWLEDGMENTS. This work was supported by the Office of Naval Research and the Department of Energy-Office of Basic Energy Sciences.

REFERENCES

1. I. Dugdale and J. GB. Cotton, *Corrosion Sci.*, 4, 397 (1964).
2. T. R. Beck, *Proceedings of International Conference on Localized Corrosion* 644 (1971), Williansburg, Va., NACE.
3. T. R. Beck, *J. Electrochem. Soc.* 120, 1317 (1973).
4. T. R. Beck, *J. Electrochem. Soc.* 120, 1310 (1973).
5. N. Casillas, S. J. Charlebois, W. H. Smyrl, and H. S. White *J. Electrochem. Soc.*, in press.
6. N. Casillas, S. R. Snyder, W. H. Smyrl, H. S. White, *J. Phys. Chem.* 95, 7002 (1991).
7. T. Ohtsuka, M. Masuda and N. Sato, *J. Electrochem. Soc.* 132, 787 (1985).
8. E. R. Scott, H. S. White and J. B. Phipps, *Solid State Ionics* 53-56, 176 (1992).
9. E. R. Scott, H.S. White and J. B. Phipps, *J. Memb. Sci.* 58, 71 (1991).
10. E. R. Scott, H.S. White and J. B. Phipps, *Anal. Chem.* 65, 1537 (1993).
11. E. R. Scott, H.S. White and J. B. Phipps, *Pharm. Res.*, in press.
12. E. R. Scott, J. B. Phipps, and H. S. White, *Science*, submitted.
13. K. Potje-Kamloth, J. Janata and M. Josowicz, *Ber. Bunsenges. Phys. Chem.* 93, 1480 (1989).
14. M.F. Abd Rabboh and P. J. Boden, *Proceedings of International Conference on Localized Corrosion* 653 (1971), Williansburg, Va., NACE.
15. J. Lausmaa, B. Kaseno, H. Mattsson, *Appl. Surf. Sci.* 44, 133 (1990).
16. C. P. Smith and H. S. White, *Anal. Chem.*, 64, 2398 (1992).
17. D. J. Smith *Proc. R. Soc. London* A391, 351 (1984).
18. D. J. Smith, L. A. Bursill, and M.G. Blanchin, *Phil. Mag* 50, 473 (1984).
19. F. Millot, M. G. Blanchin, R. Tetot, J.-F.Marucco, B. Poumellec, C. Picard, and B. Touzelin, *Proc. Solid. State. Chem.* 17, 263 (1987).

20.. G. Rohrer, V.E. Henrich, and D. A. Bonnell, *Science* 250, 1239 (1990).

FIGURE CAPTIONS

Fig. 1 Oxide growth curve for a chemically-etched Ti electrode in 0.05 M H_2SO_4. Scan rate = 1 mV/s.

Fig. 2 Schematic diagram of the scanning electrochemical microscope.

Fig. 3 Voltammetric responses of Ti electrodes as a function of oxide thickness, *t*, in a 1M KBr, 0.05 M H_2SO_4 (pH=1.05) solution. Scan rate = 1.0 mV/s.

Fig. 4 Pitting potential, E_p, versus oxide thickness, *t*, for Ti electrodes. Data were obtained from the voltammetric responses in a 1 M KBr, 0.05 M H_2SO_4 (pH =1.05) solution at a scan rate of 1 mV/s.

Fig. 5 Voltammetric responses of Ti electrodes (native oxide, $t \sim 20$Å) at 0 and 22 ^oC in a 1 M KBr, 0.05 M H_2SO_4 (pH =1.05) solution.

Fig. 6 Video micrographs showing the growth of active pits on a Ti ($t = 50$ Å) electrode immersed in a 1 M KBr, 0.05 M H_2SO_4 (pH =1.05) solution.

Fig. 7 Schematic of processes occurring during pitting corrosion of a Ti electrode in a 1 M KBr, 0.05 M H_2SO_4 (pH =1.05) solution. Dissolution of the metal yields free-standing TiO_2 films.

Fig. 8 Transmission electron micrograph of a 50 Å-thick, free-standing TiO_2 film.

Fig. 9 Schematic drawing showing the localized oxidation of Br^- on the Ti electrode and the reduction of electrogenerated Br_2 at the SECM tip.

Fig. 10 SECM images (400 x 400 μm^2) of electroactive sites on 4 different Ti electrodes ($t = 50$ Å). The electrodes were biased at: (a) 1.3 V, (b) 1.56 V, (c) 1.56 V, and (d) 1.4 V. All images were obtained at a tip-to-surface separation of ~20 µm in a 1 M KBr, 0.05 M H_2SO_4 (pH =1.05) solution. SECM-tip potential = 0.6 V. The greyscale contrast corresponds to an absolute maximum-minimum tip current range of: (a) 1.45 - 0.1 nA, (b) 0.26 - 0.07 nA, (c) 1.6 - 0.09 nA, and (d) 0.20 - 0.12 nA.

Fig. 11 SECM image (500 x 500 μm^2) of Br_2 production at a 12.5 μm-radius Pt disk. The SECM tip and Pt electrode potentials were 0.6 and 1 V vs SCE, respectively. The image was obtained in a 1 M KBr, 0.05 M H_2SO_4 (pH = 1.05) solution at a tip-to-sample separation of ~20 μm. The greyscale contrast corresponds to an absolute maximum-minimum tip-current range of 10 - 0.09 nA.

Fig. 12 SECM images of an individual electroactive site on a Ti (t = 50 Å) electrode at (a) 1.3 V, (b) 1.4 V, (c) 1.56 V, (d) and 1.56 V vs SCE. Image (d) was obtained ~40 min. after image (c). All images were obtained at a tip-to-surface separation of ~20 μm in a 1 M KBr, 0.05 M H_2SO_4 (pH =1.05) solution. SECM tip potential = 0.6 V. The greyscale contrast corresponds to an absolute maximum-minimum tip current range of: (a) 0.16 - 0.09 nA, (b) 0.18 - 0.1 nA, (c) 0.24 - 0.1 nA, and (d) 0.18 - 0.09 nA.

Fig. 13 Comparison of the potential dependence of Br_2 electrogeneration on a Ti (t = 50Å) electrode as measured from the voltammetric response and from the SECM-tip response.

Fig. 14 Schematic drawing of the proposed sequence of events occurring during the voltammetric scan of a Ti (t = 50Å) electrode in a 1 M KBr, 0.05 M H_2SO_4 solution. The shaded rectangular region within the oxide film represents a region where the electrical conductivity is large relative to the surrounding region. (a) Below the thermodynamic redox potential of the Br^-/Br_2 couple, Br^- is not oxidized at the surface. (b) Between 1.2 and 2.0 V, oxidation of Br^- occurs at microscopic surface sites. (c) Thickening of the oxide at the microscopic sites at V > 2.0 results in a decrease in the electron-transfer rate for Br^- oxidation. (d) At potentials corresponding approximately to the onset of pitting, Br chemisorption at the microscopic sites results in dissolution of the oxide and oxide breakdown. Steps (a), (b), and (c) are supported directly from voltammetric and SECM analyses. Chemisorption of Br (step (d)) and oxide dissolution is suggested by the acceleration of oxide breakdown in Br^- solutions, relative to the rate in Cl^- solutions.

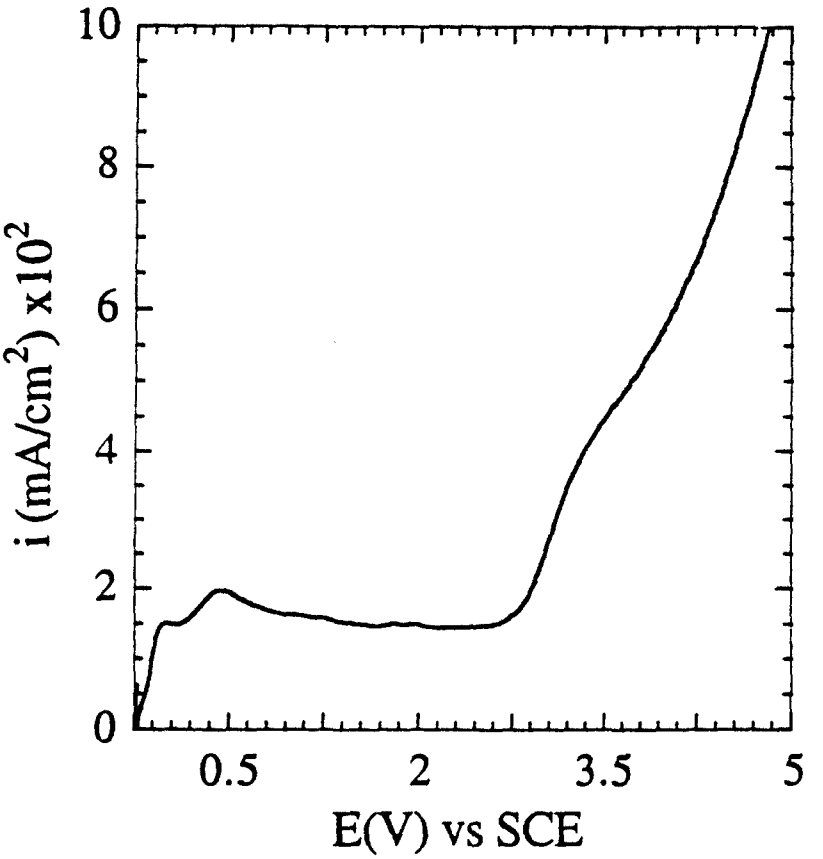

Fig 1

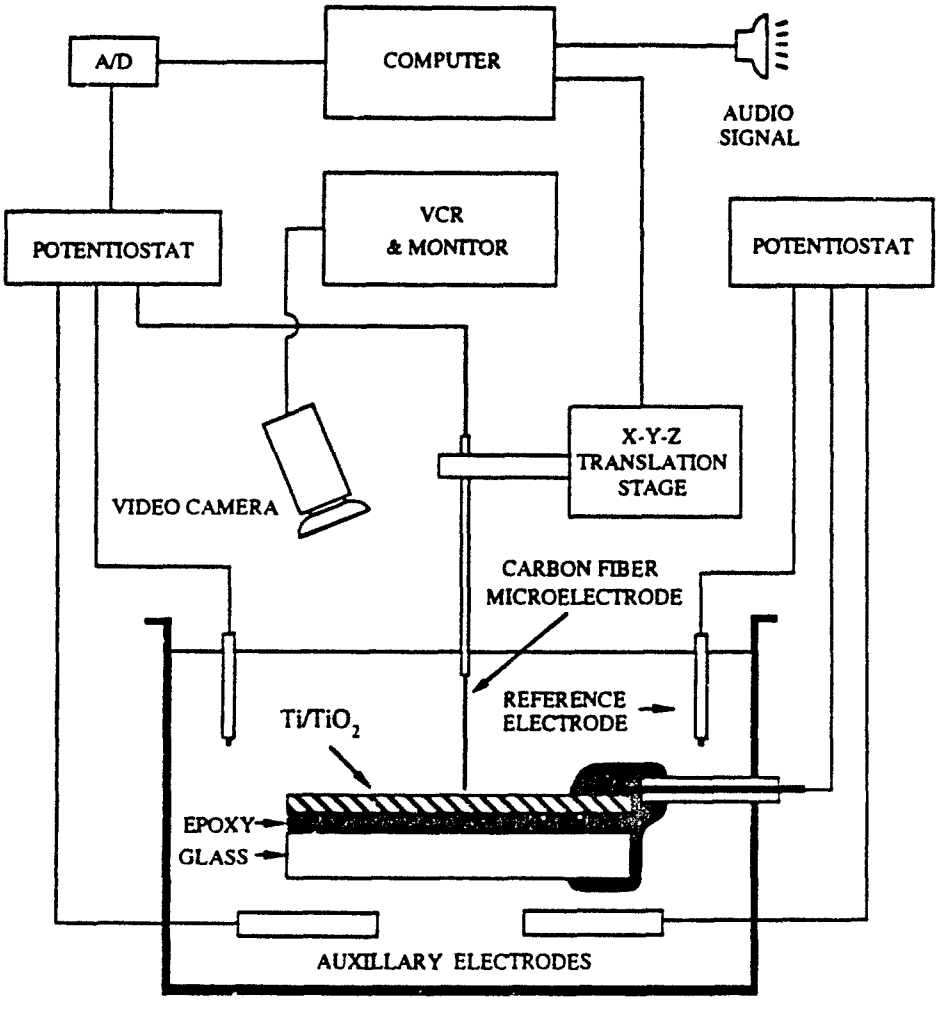
A/D
COMPUTER
AUDIO SIGNAL
POTENTIOSTAT
VCR & MONITOR
POTENTIOSTAT
X-Y-Z TRANSLATION STAGE
VIDEO CAMERA
CARBON FIBER MICROELECTRODE
REFERENCE ELECTRODE
Ti/TiO2
EPOXY
GLASS
AUXILLARY ELECTRODES

Fig 2

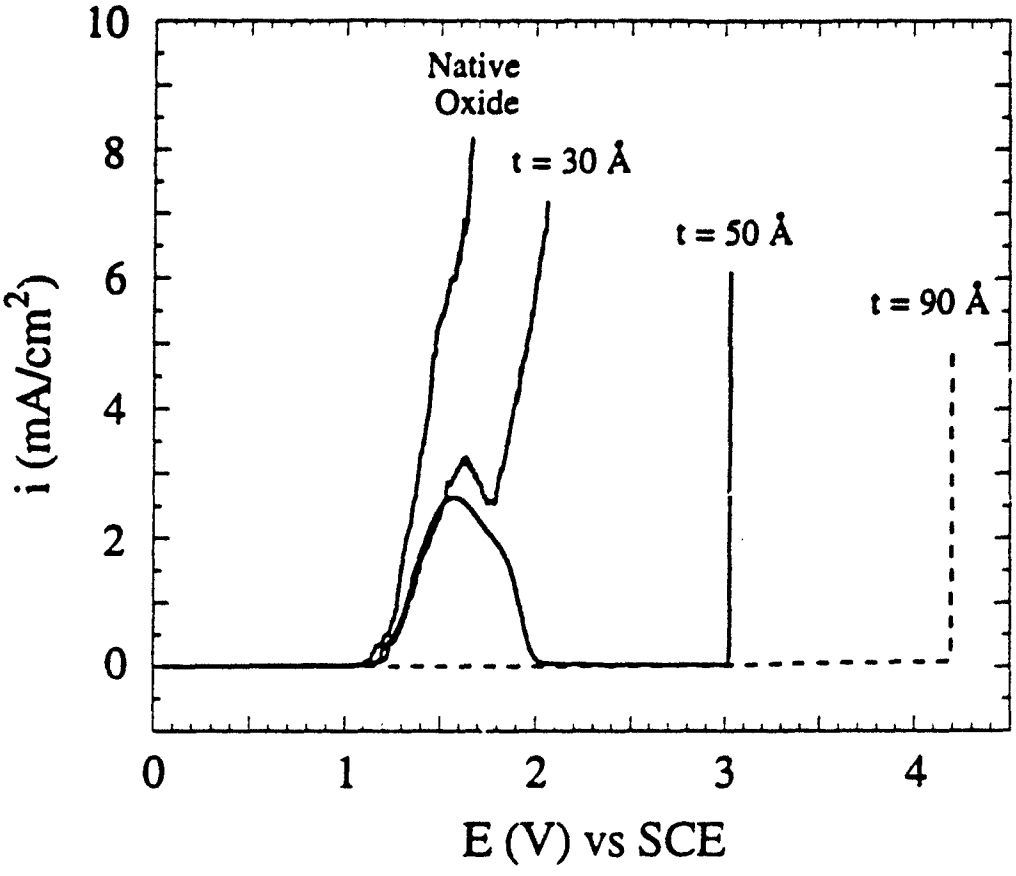

Fig 3

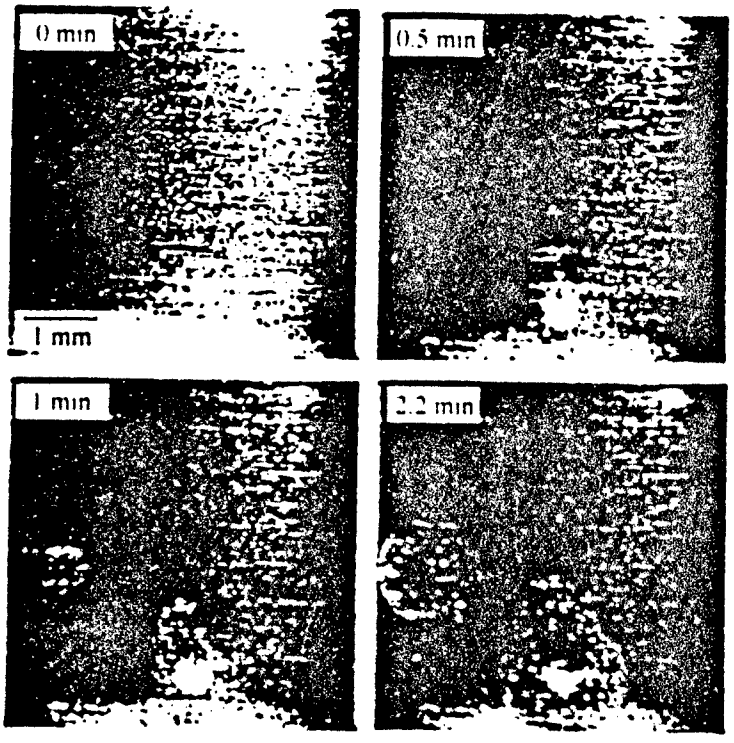

Fig 4

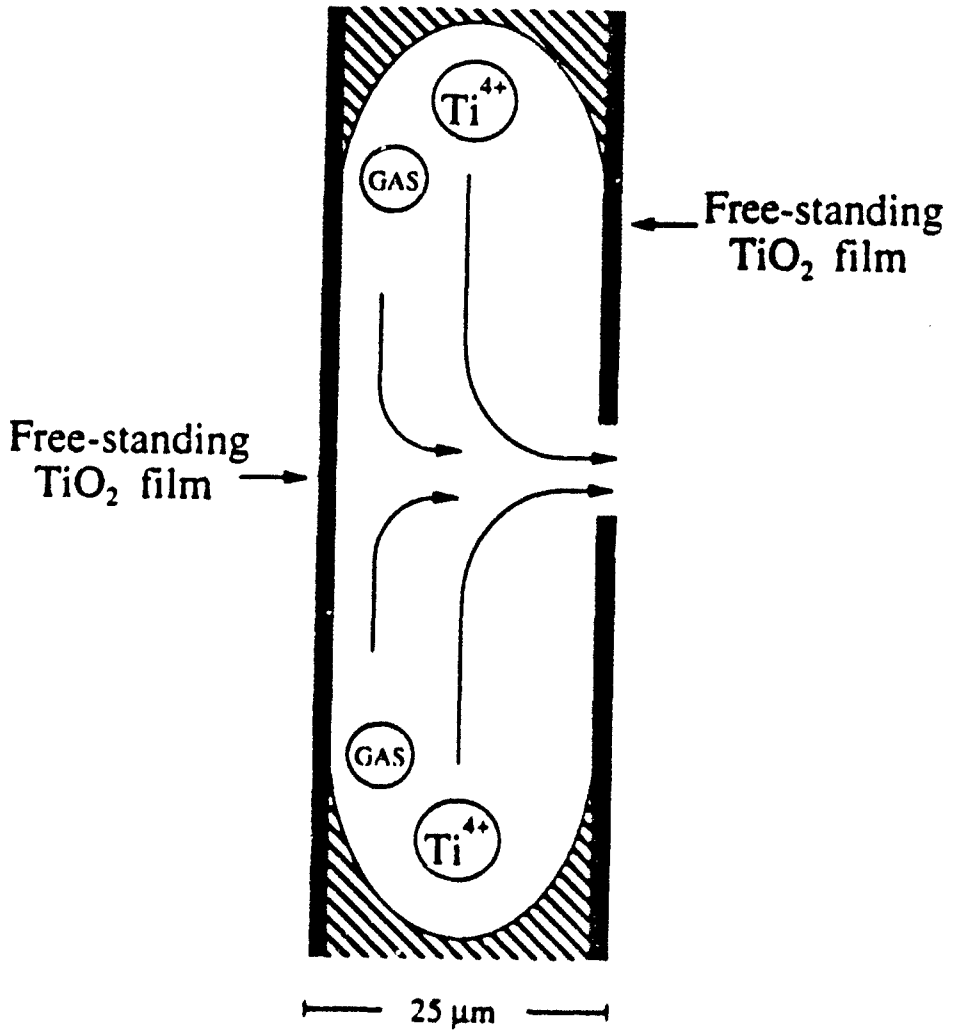
Ti4+
GAS
Free-standing
TiO2 film
Free-standing
TiO2 film
GAS
Ti4+
25 µm

Fig 5

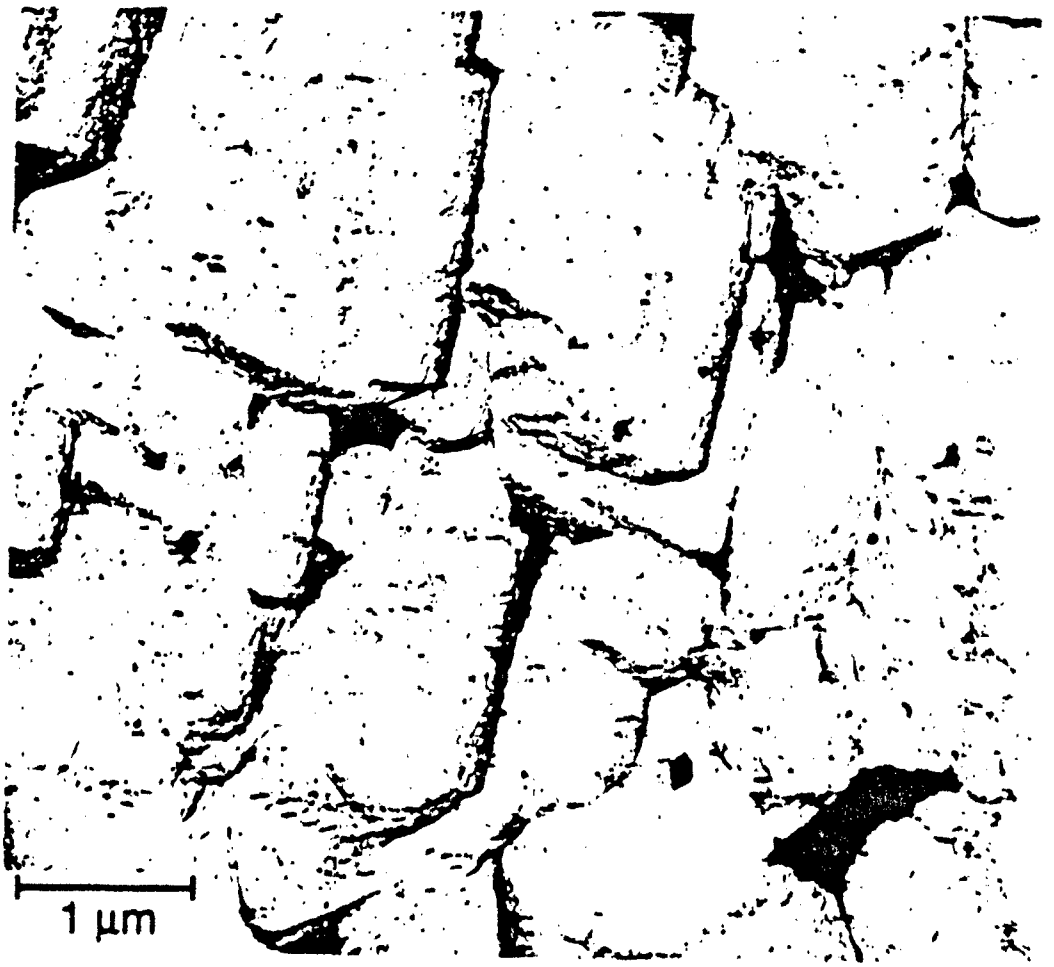

Fig 6

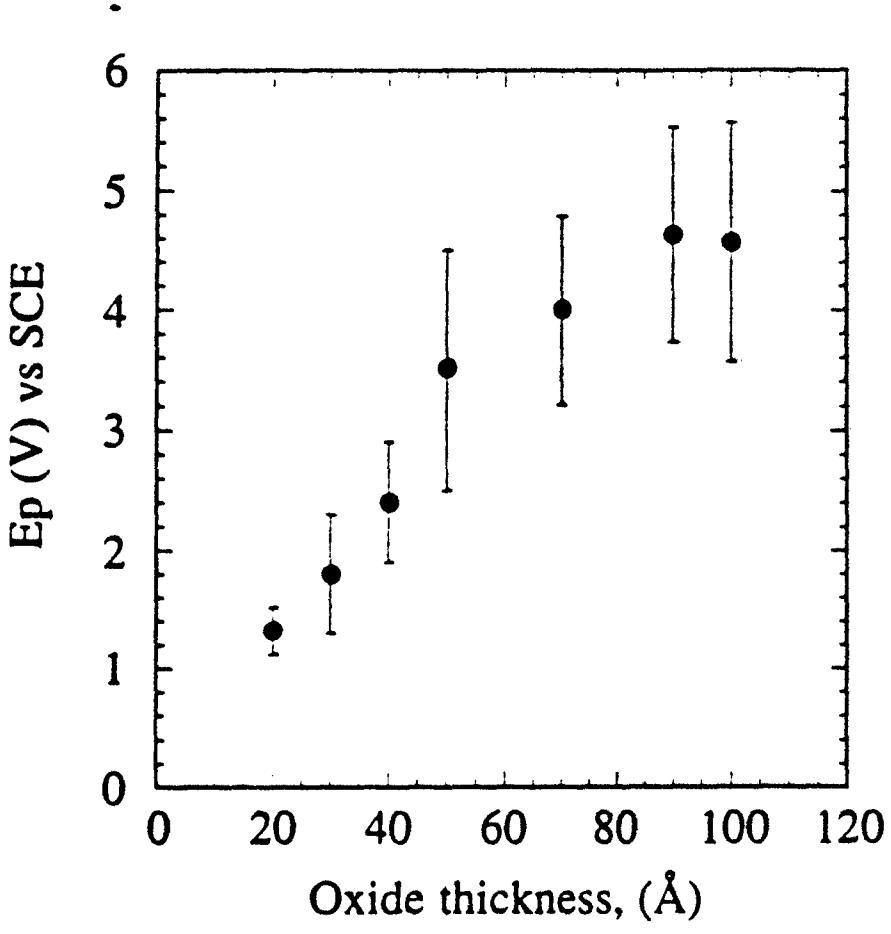

Fig 7

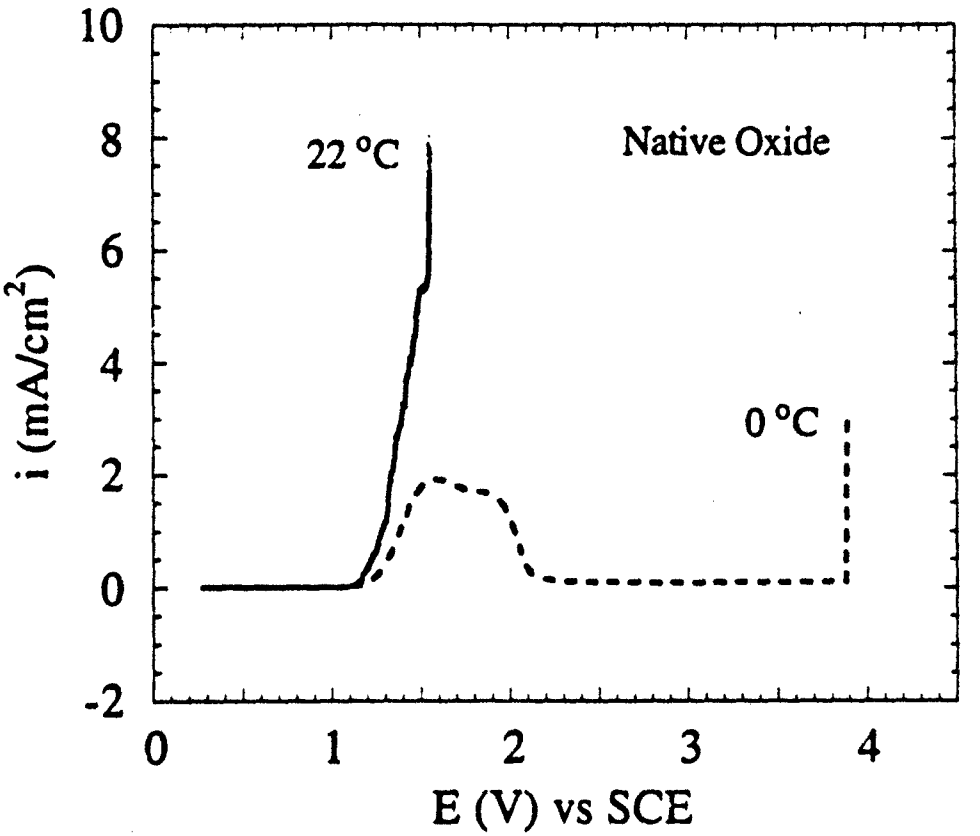

Fig 8

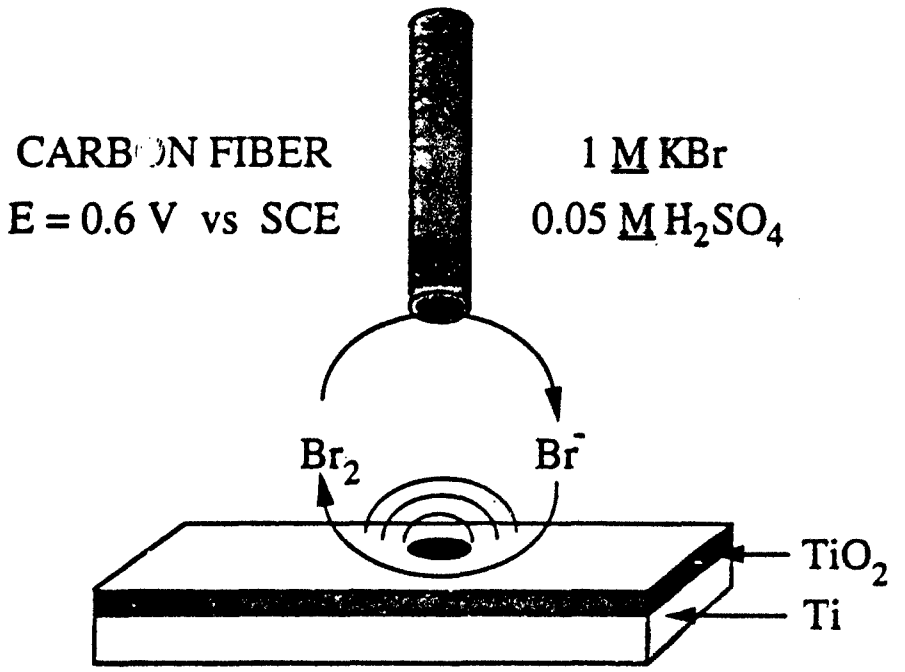

$1.2 \leq E \leq 2.0$ V vs SCE

Fig 9

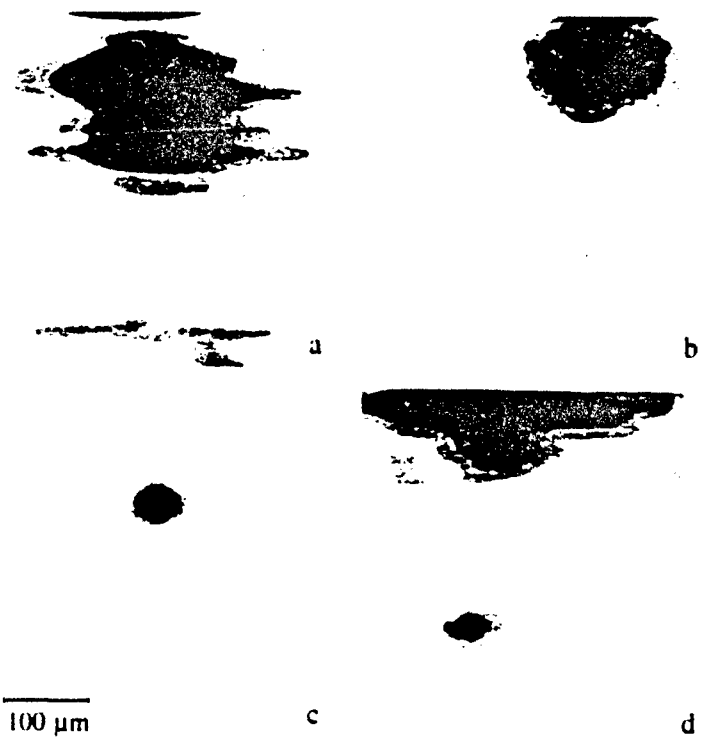

Fig 10

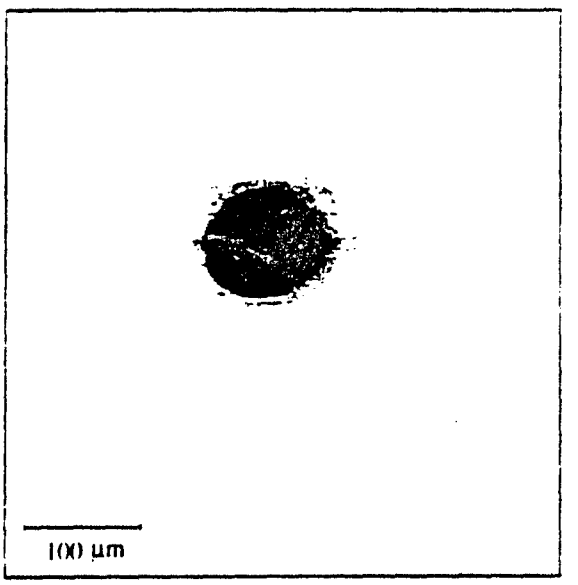

Fig 11

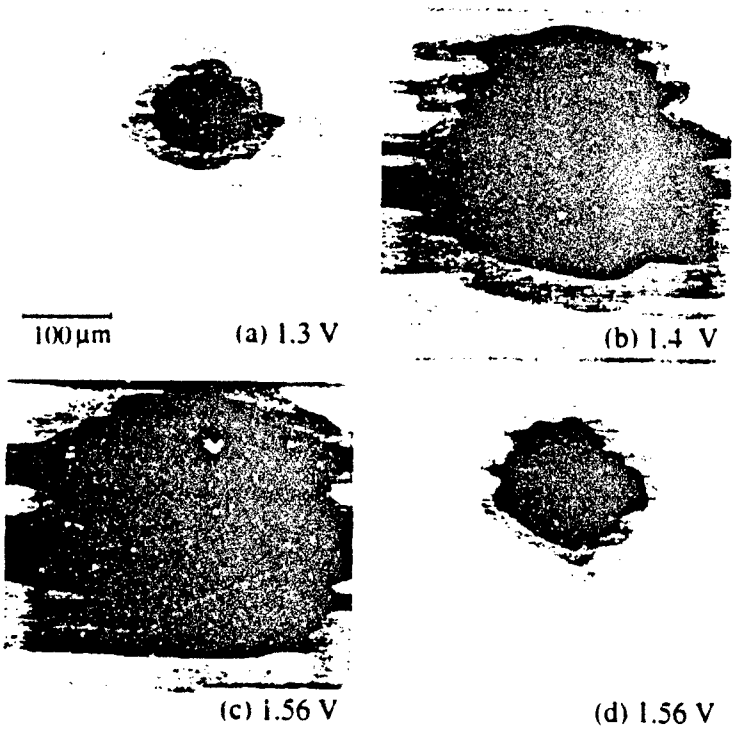

Fig. 12

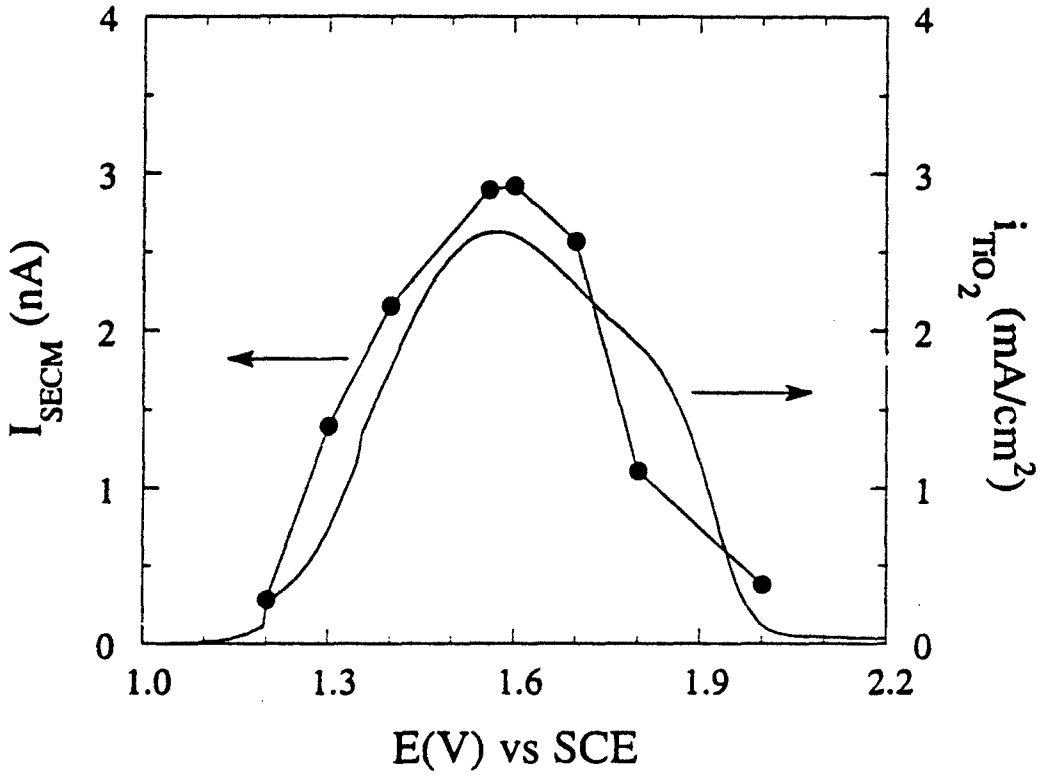

Fig. 13

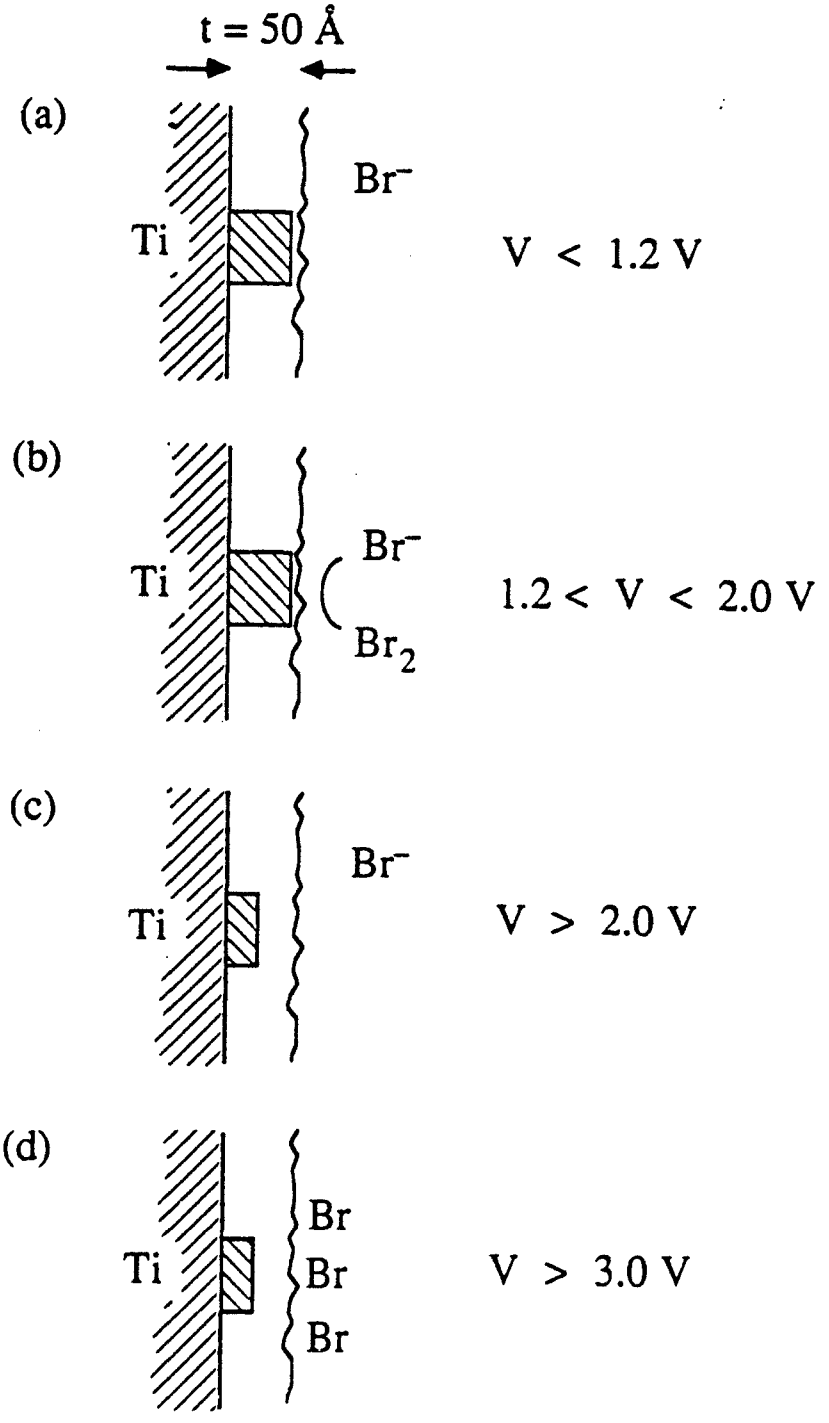

Fig 14